Targeting Unoccupied Surfaces on Protein-Protein Interfaces

David Rooklin,[†‡] Ashley E. Modell, [†‡] Haotian Li, [†] Viktoriya Berdan, [†] Paramjit S. Arora[†]* and Yingkai Zhang[†⊥]*

†Department of Chemistry New York University, New York, NY 10003, U.S.A and ⊥ NYU-ECNU Center for Computational Chemistry, New York University–Shanghai, Shanghai, China

Supporting Information

Table of contents **Page**

Molecular images were generated with the UCSF Chimera package.[1]

Details of computational design and simulations

The workflow for our approach included: 1. Assessment of multiple PDB structures of the KIX/MLL complex in order to characterize two distinct pocket states utilized by MLL and determined by the ternary complex state of the system; 2. Selection of the pocket state more amenable to optimization due to the identification of high scoring underutilized pocket space adjacent to the helical motif; 3. Use of alpha-clusters as a physical representation of targetable pocket space to guide the selection of natural and non-natural amino acid mutations able to enhance pocket-ligand complementarity across the interface; 4. Molecular dynamics simulation to evaluate complex structure and stability.

1. Using AlphaSpace, we mapped 40 PPI interfaces from 2 solution state NMR structures: the KIX/MLL dimer state (PDB:2LXS) and the CMyb/KIX/MLL trimer state (PDB:2AGH).[2,3] We applied the *Pocket Matching* approach, introduced in ref [4], to cluster similar localized pockets across the set of KIX/MLL conformations and to calculate ensemble average pocket scores for each pocket cluster (Figure 1A,B and Figure S1). The set of pockets to be clustered was selected based on proximity to the MLL peptide, using a 1.6 Å "contact" distance between any atom in the peptide and any alpha-atom from the pocket. Pocket clustering is performed using the average linkage algorithm on the *Jaccard* distance matrix. Pairwise pocket distances are calculated between binary arrays of length *n,* where *n* is the number of heavy atoms in the protein, and each value is *1* if the corresponding atom is pocket lining and *0* if not. The *Pocket Matching* result reveals a clear bimodal surface state between the KIX/MLL dimer and the CMyb/KIX/MLL trimer. Each state has 7 primary pocket clusters at the interface. Among these clusters, only 2 are shared across the two pocket states, thus each state has 5 unique pocket clusters.

2. Pocket score is calculated as the non-polar alpha-space volume, as described in ref [4]. Pocket occupation is calculated at the alpha-atom resolution. Each alpha-atom is designated as occupied (i.e. at least one peptide atom within 1.6 Å) or otherwise as unoccupied. High scoring unoccupied pocket space indicates an opportunity to enhance local surface contact at the interface. To calculate occupied pocket space by MLL residue, each occupied alpha-atom is associated with the nearest residue from MLL, and the associated alpha-space volumes are summed for each residue. AlphaSpace analysis reveals that each pocket state exhibits 2 high scoring pockets, two moderate scoring pockets, and 3 low scoring pockets. The highest scoring pocket, in both pocket states, is associated with MLL residue F^{852}, however the location of the second high-scoring pocket differs between states. In *Pocket State 1*, the second high scoring pocket is adjacent to the N-terminal strand region of MLL, and is highly occupied by strand residue L^{845}. In *Pocket State 2,* the second high scoring pocket is identified to be near the C-terminal end of the helical region, and only partially occupied by helix residue Y^{857}. In addition to this high scoring underutilized targetable pocket, the moderate scoring pocket occupied by L^{845} in *Pocket State 2* is targetable by an extension from the M^{850} position. In conjunction, these pocket opportunities and the reduced pocket occupation by strand residues make *Pocket State 2* more amenable toward optimization of the helical motif.

3. The structure PDB:2AGH.1 was selected for design based on high-scoring unoccupied pocket space near M^{850}, V^{853}, F^{852}, and Y^{857}. Alpha-clusters represent the general shape of the accessible pocket space and their visualization can be used to guide the selection of natural or non-natural

amino acids from the SwissSidechain database.[5] The rational design strategy is to select for mutations in the peptide such that percentage pocket occupation is enhanced while avoiding the introduction of steric clashes with the KIX surface. Percentage pocket occupation is calculated as the sum of the alpha-space volumes associated with occupied alpha-atoms over the total pocket alpha-space volume (Figure 3). Residues were selected by hand and pocket occupation was evaluated using AlphaSpace. In targeting pocket 3, benzyl-cysteine was selected as a particularly long residue to replace M^{850} in order to reach the pocket space unoccupied by the truncation of L^{845}, and $V^{853}I$ was then selected to hit the remaining unoccupied alpha-atoms between the two residues. For pocket 2, the high-scoring unoccupied pocket near the C-terminus of MLL, the pocket was observed to be broad and flat, similar to a phenyl ring structure, and Tyr was selected over Phe to complement the polar atoms observed toward the back of the pocket. Lastly, while the native F^{852} exhibits good occupation of pocket 1, the associated alpha-cluster reveals a small set of unoccupied alpha-atoms near the base of the residue that is targetable from the 2-position of the ring, and we selected 2-methyl-phenylalanine to enhance pocket occupation to 100%. A more automated and systematic screening of all residues in the database is now under development and may provide alternatives to these residues selected by hand. However, for this initial proof-of-concept application, we want to highlight the simplicity and intuitiveness of our side chain selection strategy. The selected mutations—M^{850}>Bcs (benzyl-cysteine), F^{852}>2mf (2-methyl-phenylalanine), V^{853}>Ile, T^{857}>Tyr—and pocket occupation analysis are illustrated in Figure 2.

4. Extensive molecular dynamics simulation was performed to compare the stability and structure of 3 complex systems: KIX/MLL-WT, KIX/MLL1, and KIX/MLL6. For all systems, IAPP and MLL protein coordinates were taken from PDB:2AGH.1 (with c-Myb removed), with respective modifications to the MLL peptide made using the UCSF Chimera package.[6] The starting structure is selected from *Pocket State* 2 in order to observe its stability in the absence of c-Myb and to evaluate and compare potential peptide-protein interactions specifically against *Pocket State* 2. The Amber14 molecular dynamics package[7] was used for all minimization and simulation, employing the Amber14SB force field[8] for the KIX protein and for the natural residues in the MLL peptide. Force field parameters for non-natural amino acids (benzyl-cysteine and 2-methyl-phenylalanine) were obtained from Forcefield_NCAA.[9] Systems were neutralized with either Na^+ or Cl^- counterions and solvated using the explicit TIP3P water model to fill a rectangular periodic box with 10.0 Å buffer using the *tleap* module within AmberTools 15. Each solvated systems comprises ~24 000 atoms. The Particle-Mesh Ewald method with 12.0 Å cutoff was applied to treat non-bonded interactions. After a series of restrained minimizations and equilibrations (see [10] for details), standard NPT ensemble molecular dynamics simulations were performed using the CUDA version of PMEMD (Particle Mesh Ewald Molecular Dynamics).[11,12] The SHAKE algorithm was applied to constrain bonds involving hydrogen. A time step of 2 fs was used with the Berendsen thermostat to control the system temperature at 300 K. Default values were used for all other parameters. Five 350 ns simulations (using different initial velocities) were generated for each system. The first 50 ns of each simulation are used for unrestrained equilibration, and snapshots were saved every 1 ns from the final 300 ns for analysis. We observed the specific interactions associated with *Pocket State 2* to be generally stable throughout the duration of the 300 ns in all 5 MLL-WT simulations and in 4 out of 5 MLL-6 simulations, however the local interactions for MLL-1 were not conserved between simulations, as illustrated in Figure S3.

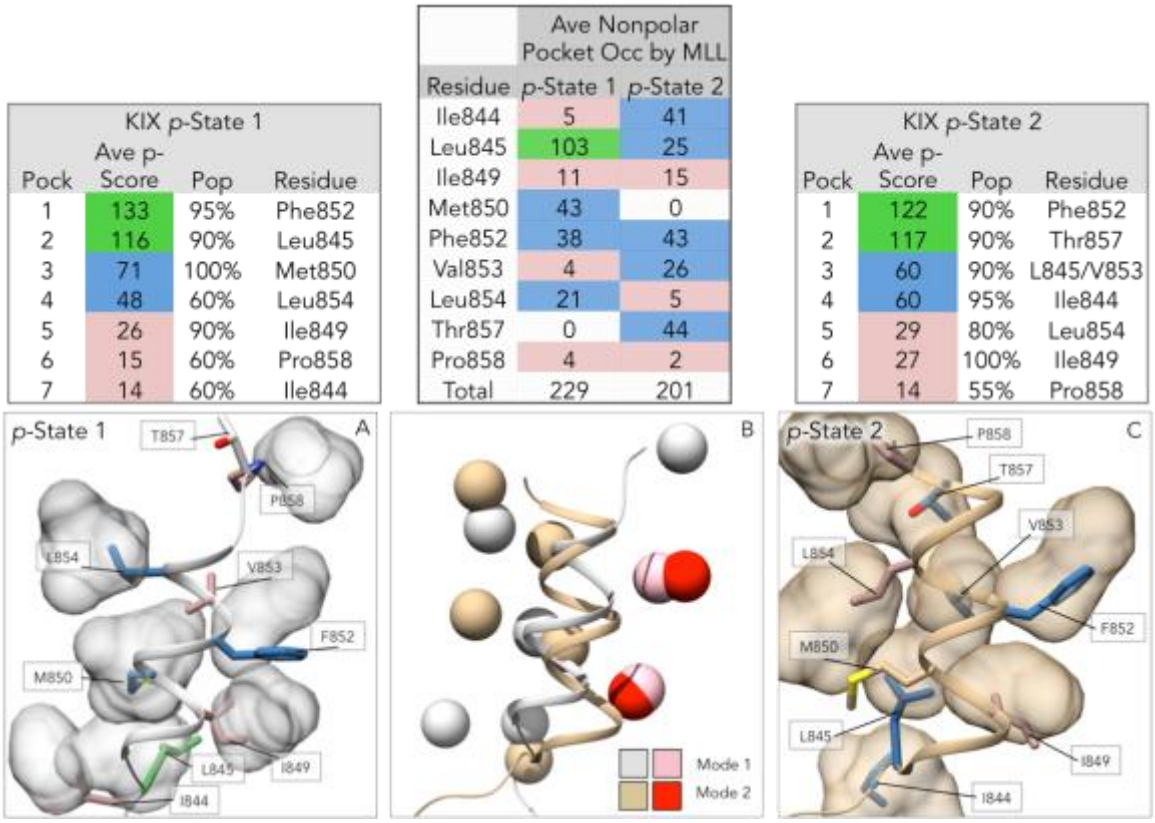

Fig S1. Upper tables on the left and right list the properties for pocket clusters from *Pocket State 1* and *Pocket State 2* of KIX/MLL: average pocket score (>100 green, >30 blue, <30 pink), population of snap shots where pocket is detected, and the MLL residue associated with each pocket. The top center table lists average nonpolar pocket occupation by MLL residue for each pocket state (>100 green, >20 blue, <20 pink). In panels (A) and (C), surface representation outlines each cluster of pocket centers to illustrate the localization of each pocket cluster. Residues from MLL are labeled and colored according to their respective average nonpolar pocket occupation. In (B), the representative structures from *Pocket State 1* and *Pocket State 2* are superimposed along with the pocket cluster centroids to illustrate the spatial modulation of pocket clusters between the pocket states. The two pairs of pink and red spheres indicate pocket clusters that "match" between the pocket states due to similar sets of pocket lining atoms. All other pocket clusters are unique to their respective binding mode.

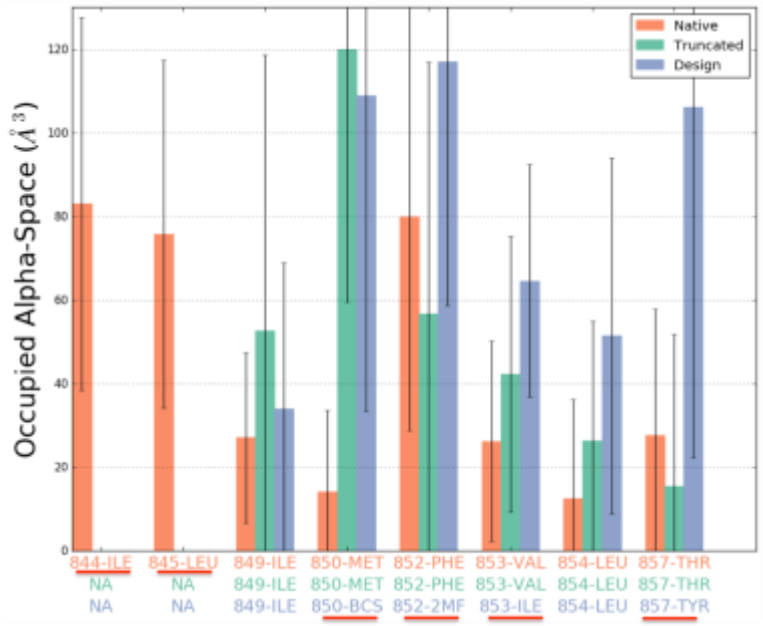

Fig S2. Average pocket occupation by residue from MD simulation of the wild type full-length MLL peptide (orange), the wild type truncated peptide—MLL1 (green), and the fully optimized peptide—MLL6 (blue). For each system, average values are calculated over 5 independent 300 ns simulations. Red underscores highlight the important strand residues from the wild type MLL and the 4 optimized residues in MLL6. Note: While Met^{850} (Truncated) and Bcs^{850} (Design) exhibit similar pocket occupation independently, Met^{850} achieves this through a global rotation of the helix into the pocket evacuated by the truncation of Leu^{845}, and this indirectly compromises the pocket occupation of other residues (e.g. Phe^{852}, see Figure S3).

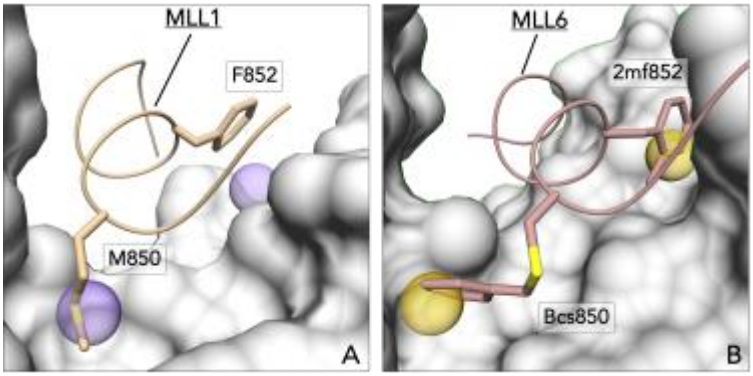

Fig S3. Representative structures from molecular dynamics simulation of KIX/MLL1 (A) and KIX/MLL6 (B) with pocket centroids represented as colored spheres. Highlighted here is the mechanism by which Met^{850} can achieve high pocket occupation in the truncated MLL1. However, the global shift of the entire MLL1 helix compromises the pocket occupation of other key residues, especially Phe^{852}. (B) Alternatively, the longer and bulkier side chain of Bcs^{850} in the designed MLL14 extends to achieve high pocket occupation while preserving the native position and high pocket occupation of $2mf^{852}$.

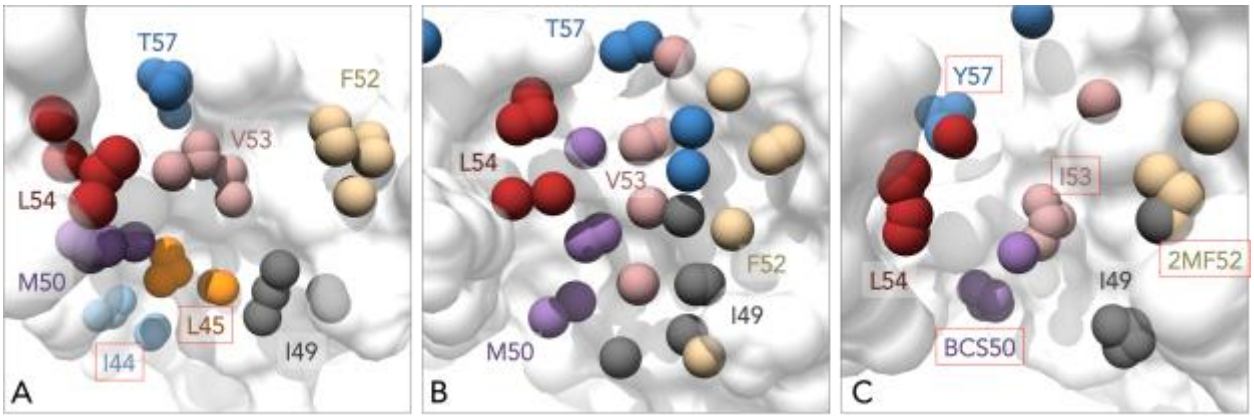

Fig S4. Average position of residue-occupied pockets to compare the binding modes from 5 independent KIX simulations for each of three systems: (A) MLL-WT, (B) MLL1, and (C) MLL6. For each snap shot, all pocket space at the interface is associated with the nearest residue from MLL. Each sphere represents the geometric center for a residue-occupied pocket cluster from one 300 ns simulation and is color coordinated and labeled by the associated residue from MLL. In (C), optimized residues are highlighted with red boxes.

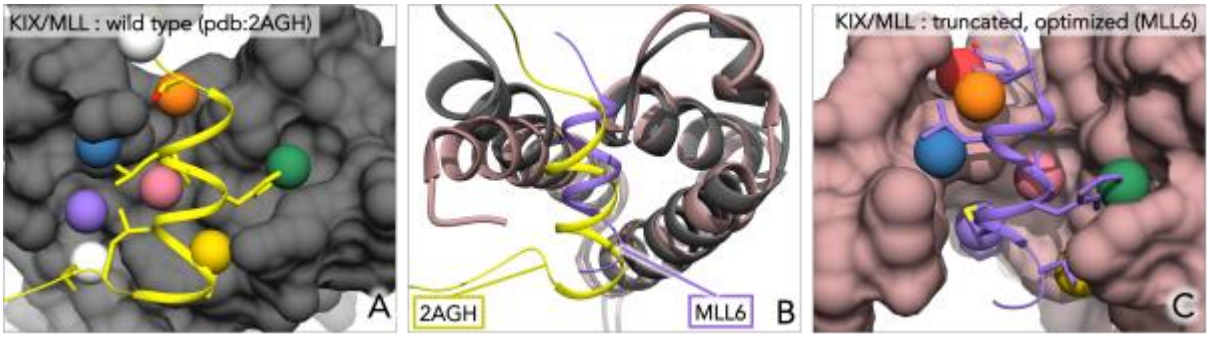

Fig S5. Illustration of the conformational modulation between the wild type full length MLL in *Binding Mode 2* from PDB:2AGH (A) and the binding mode observed in 4 out of 5 molecular dynamics simulations for the optimized peptide MLL6 (C), with respective representative structures superimposed in panel (B) showing the helix tilt of MLL6 (pink ribbon) that opens the "gap" within the helix bundle of KIX. Pocket cluster centers are represented as large spheres, with similar pockets color coordinated between (A) and (C) to highlight the enhanced spatial complementarity between residues and pockets for MLL6. A deep pocket (red) is observed only for MLL6 (C) and accommodates the important T^{857}>Y mutation.

Materials:

Commercial grade solvents and reagents were used without further purification. All amino acids and amino acid analogues were purchased from ChemImpex. Resins were purchased through EMD Millipore or VWR. Reagents and solvents were purchased through VWR unless otherwise noted.

Plasmids used in this paper were generously shared by Will Pomerantz (U. Minnesota).

Methods: Synthesis, Purification and Characterization of Peptides

Solid-Phase Peptide Synthesis:

Rink amide resin (0.80 mmol/g) was used to yield peptides with c-terminal amines. Pre-loaded fmoc-L-proline-2-chlorotrityl resin (0.36 mmol/g) was used to yield peptides with c-terminal acids. All peptides were synthesized using standard Fmoc-solid phases synthesis on a CEM® Liberty Peptide Synthesizer. The deprotection solution (20% Piperidine/DMF) was supplemented with 0.1 M HOBt to prevent aspartimide formation. [13]

Addition of Fluorescein:

Fluorescein-labeled peptides were synthesized on the peptide synthesizer through the Fmoc-βAlanine. After removal from the synthesizer and deprotection of the Fmoc group, 1.2 eq. of fluorescein isothiocyanate (FITC) and 2 eq. of DIEA in DMF were added to the peptide on resin for 2 hours at room temperature (see Fig. S5). Resin washes were performed in between steps with DMF, DCM, MeOH, DMF, DCM with 5 column volumes each. The addition of FITC was monitored via MALDI-TOF.

Cleavage and Purification of Peptides:

All peptides were cleaved from the resin and globally deprotected by applying a solution of 90% trifluoroacetic acid, 5% thioanisole, 3% 1,2-thanedithiol, 2% anisole to the resin for 1.5 - 2 hours at room temperature. The resin was filtered and the peptide was concentrated in vacuo before preiciptation with cold diethyl ether. The crude peptides were dried under nitrogen before reversed-phase HPLC using C-18 columns. A 5-75% gradient of acetonitrile in water supplemented with 0.1% TFA over 60 minutes was used. Each peptide was lyophilized and yielded a white to off-white powder in 40-50% yield depending on sequence. Purity of the compounds were checked using an LCMS-Single Quad column run with 5-95% acetonitrile in water with 0.1% formic acid over 10-11 minutes. Exact masses were determined using the Bruker UltraFlex MALDI-TOF (Table S1).

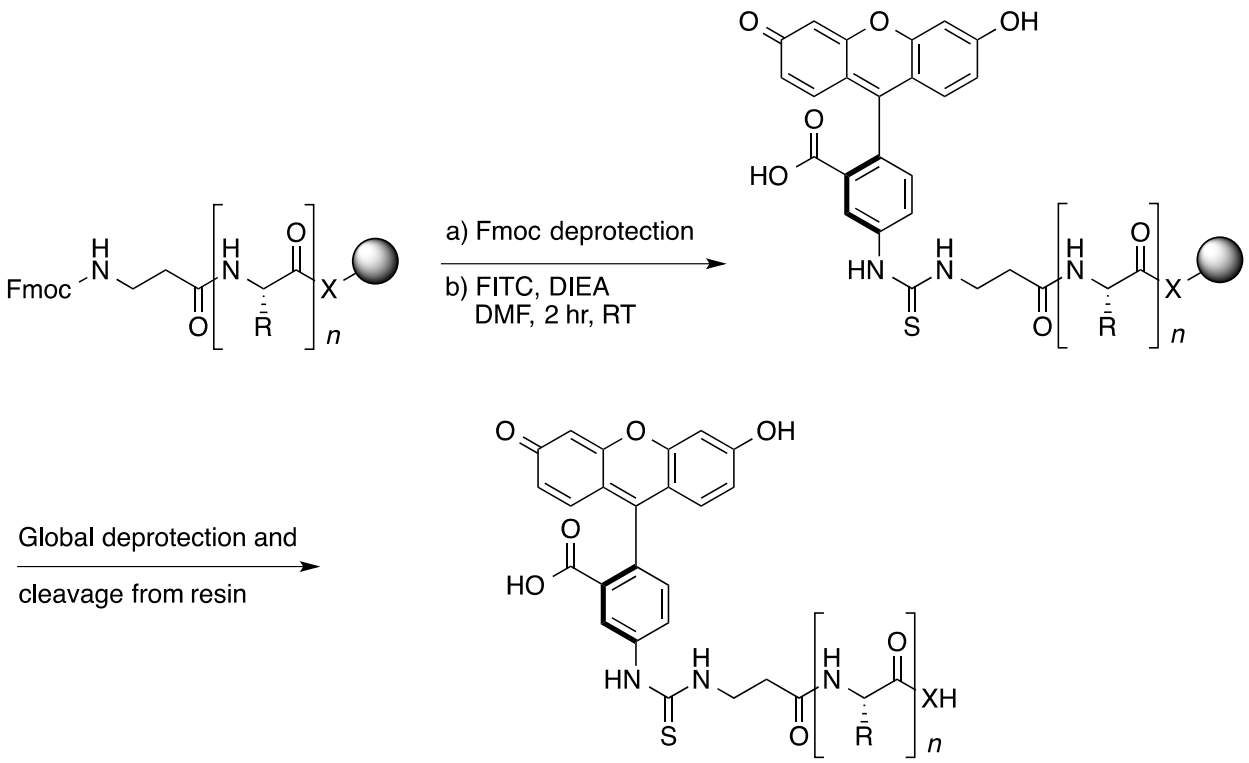

Fig S6. Synthesis of fluorescein-labeled peptides. For Rink Amide Resin X = NH; for 2-chlorotrityl resin X = O.

Table S1. Compound Characterization

Compound	Sequence	$[M+H]^+$ Calc'd	$[M+H]^+$ Found
WT-MLL^{Flu}	Flu-βA-DCGNILPSDIMDFVLKNTP-NH_2	2551.0906	2552.7927
MLL1^{Flu}	Flu-βA-SDIMDFVLKNTP-NH_2	1838.7691	1839.1352
MLL2 ^{Flu}	Flu-βA-SDIC*DFVLKNTP-NH_2	1900.7848	1901.3984
MLL3 ^{Flu}	Flu-βA-SDIC*DFVLKNYP-NH_2	1962.8004	1963.1553
MLL4 ^{Flu}	Flu-βA-SDIC*DFILKNYP-NH_2	1976.8161	1976.8338
MLL5 ^{Flu}	Flu-βA-SDIC*DFILKNYP-OH	1977.8001	1978.0058
MLL6 ^{Flu}	Flu-βA-SDIC*DF*ILKNYP-OH	1991.8158	1992.2790
WT-MLL	Ac-DCGNILPSDIMDFVLKNTP-NH_2	2133.0282	2133.2525
MLL1	Ac-SDIMDFVLKNTP-NH_2	1420.7068	1420.8940
MLL2	Ac-SDIC*DFVLKNTP-NH_2	1482.7225	1482.9416
MLL3	Ac-SDIC*DFVLKNYP-NH_2	1544.7381	1544.9192
MLL4	Ac-SDIC*DFILKNYP-NH_2	1558.7538	1558.9713
MLL5	Ac-SDIC*DFILKNYP-OH	1559.7378	1559.8728
MLL6	Ac-SDIC*DF*ILKNYP-OH	1573.7534	1573.6146
C*→A	Ac-SDIADF*ILKNYP-OH	1451.7344	1451.8265
F*→A	Ac-SDIC*DAILKNYP-OH	1483.7065	1483.8544
I→A	Ac-SDIC*DF*ALKNYP-OH	1531.7065	1531.8681
Y→A	Ac-SDIC*DF*ILKNAP-OH	1481.7272	1481.6718
OH→NH_2	Ac-SDIC*DF*ILKNYP-NH_2	1572.7694	1572.6368

All single letter amino acid codes are used above in addition to the following abbreviations:
Flu = fluorescein
βA = β-alanine
Ac = acyl cap
C* = beznyl-cysteine
F* = 2-methyl-phenylalanine
WT-MLL^{Flu} sequence is the same used in Majmudar, C.Y., *et al.* [14]

Analytical HPLC Traces of Purified Peptides

WT -MLL^{Flu}

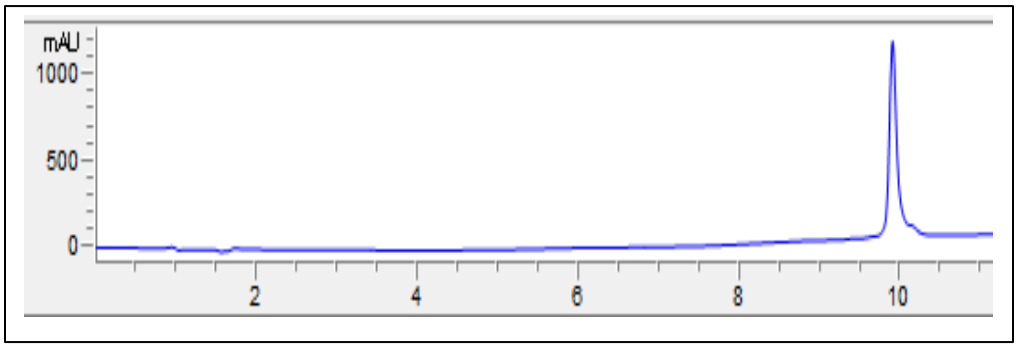

MLL1^{Flu}

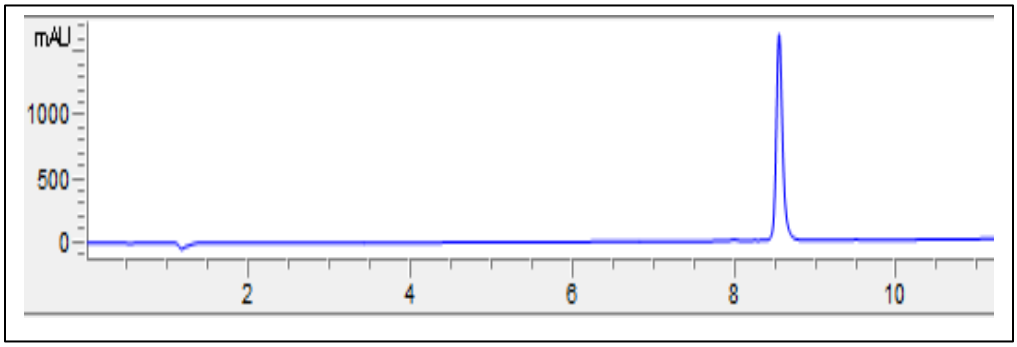

MLL2^{Flu}

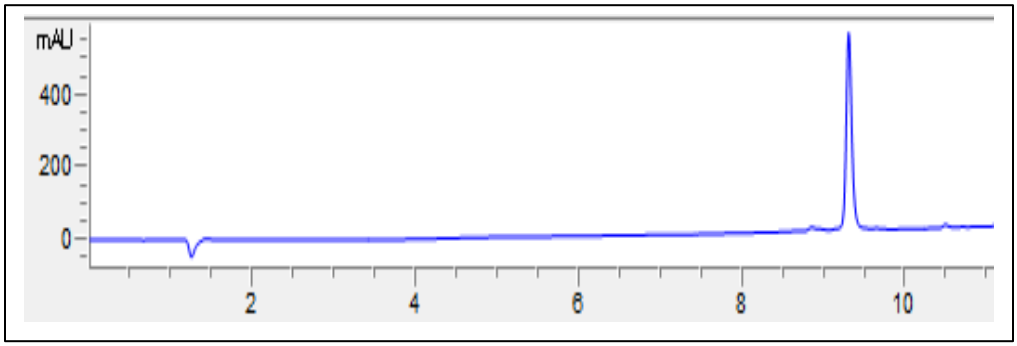

MLL3^{Flu}

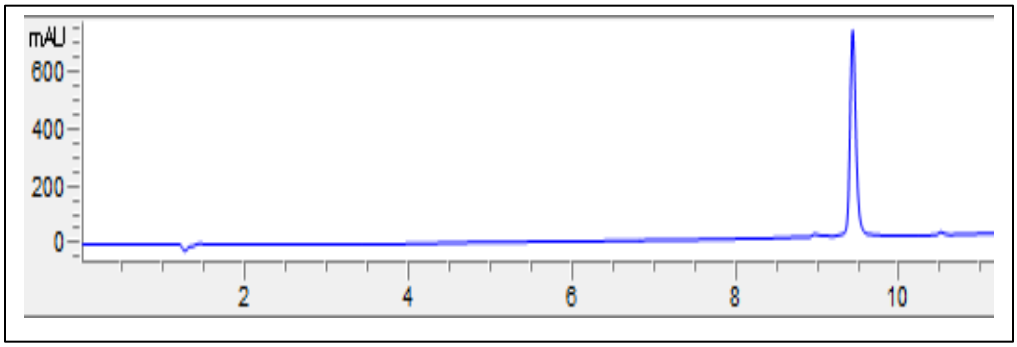

MLL4^{Flu}

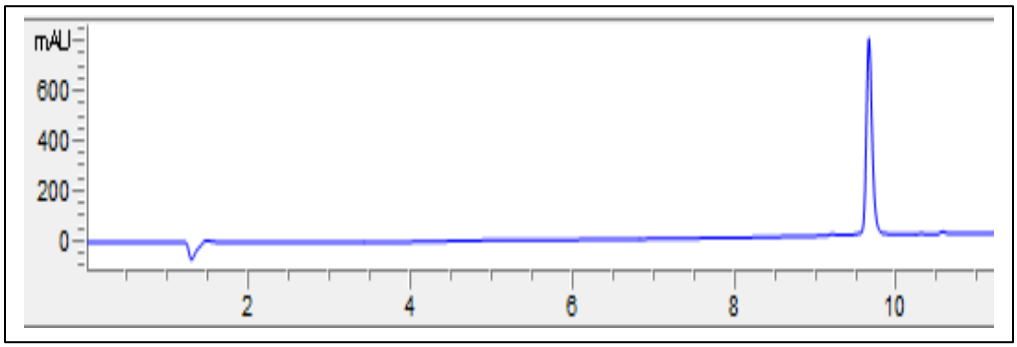

MLL5^{Flu}

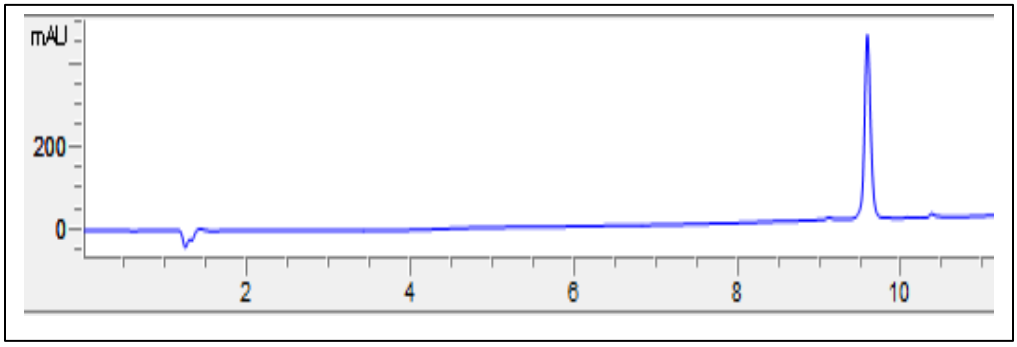

MLL6^{Flu}

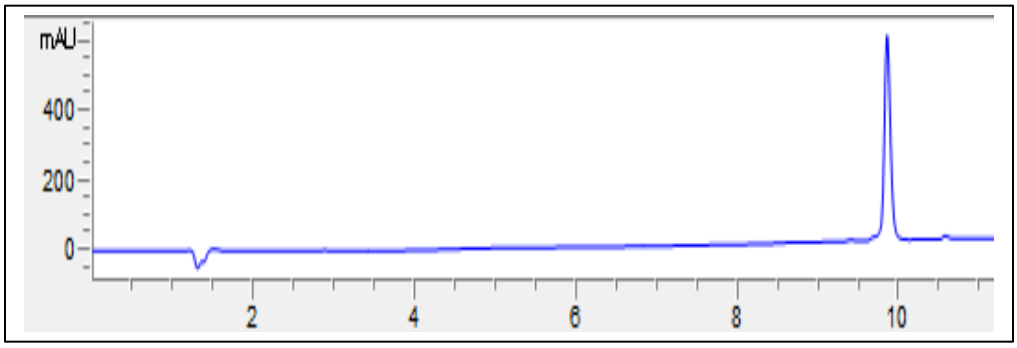

WT-MLL

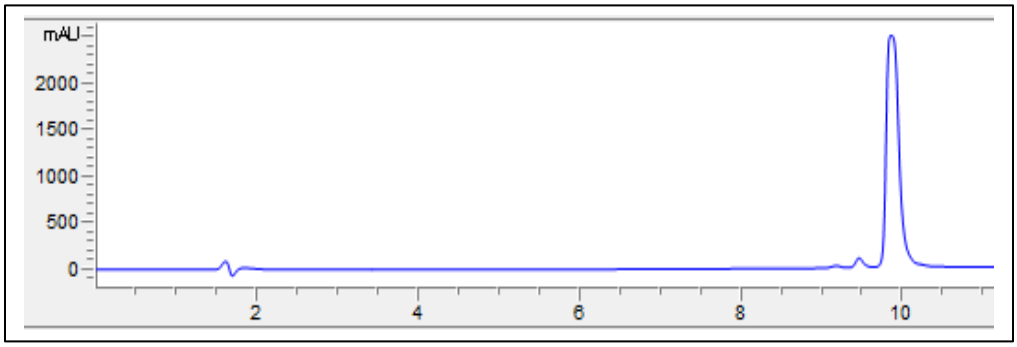

MLL1

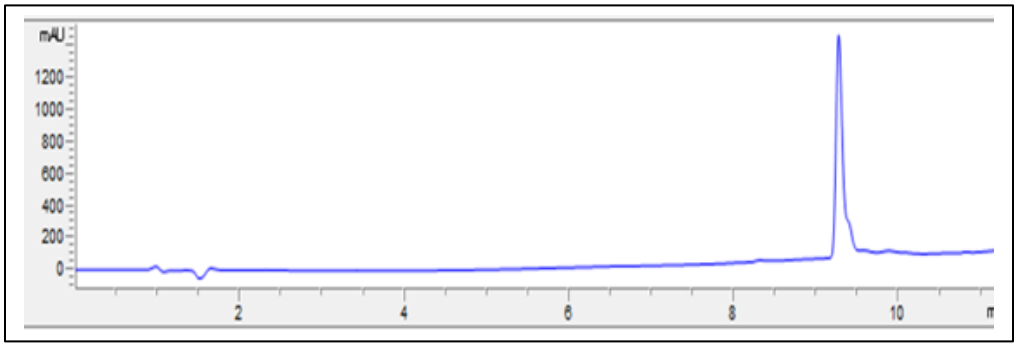

MLL2

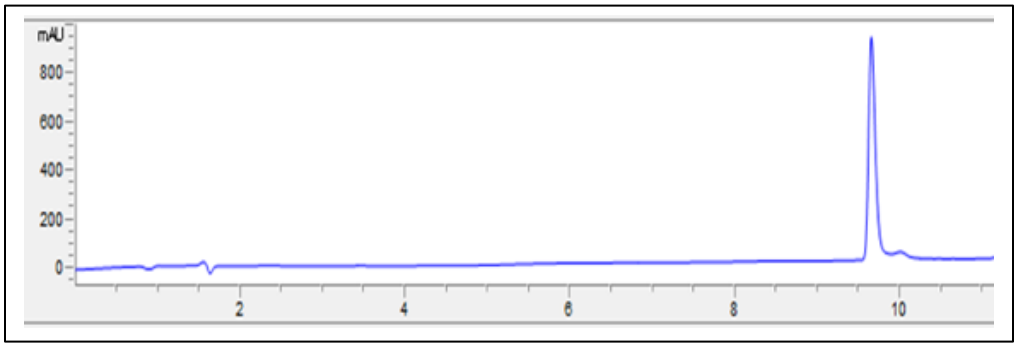

MLL3

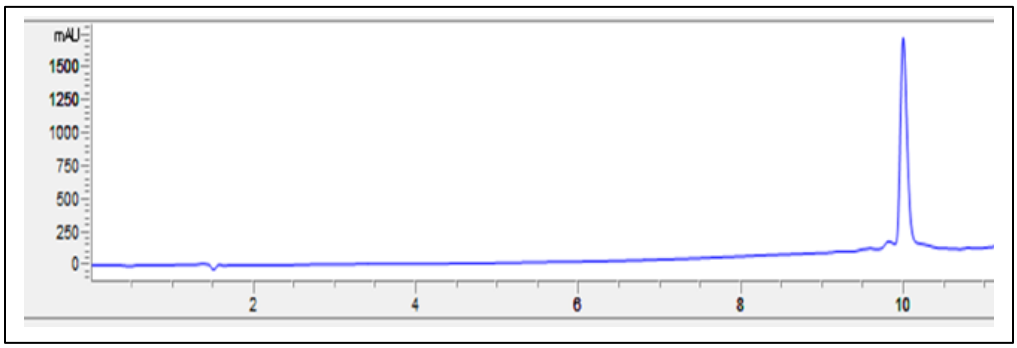

MLL4

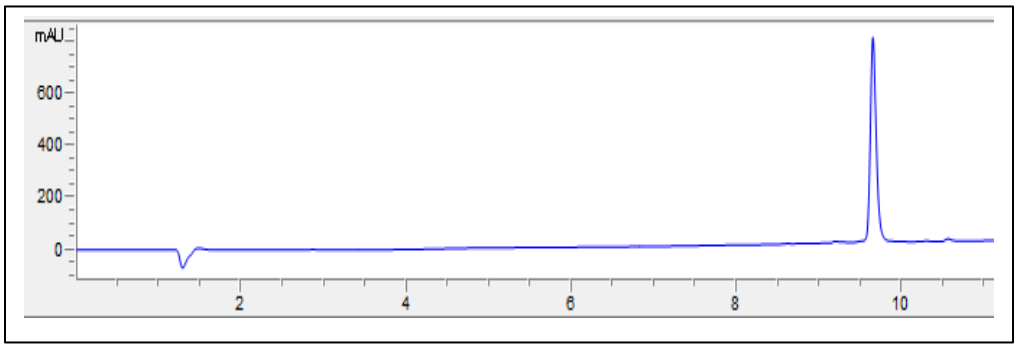

MLL5

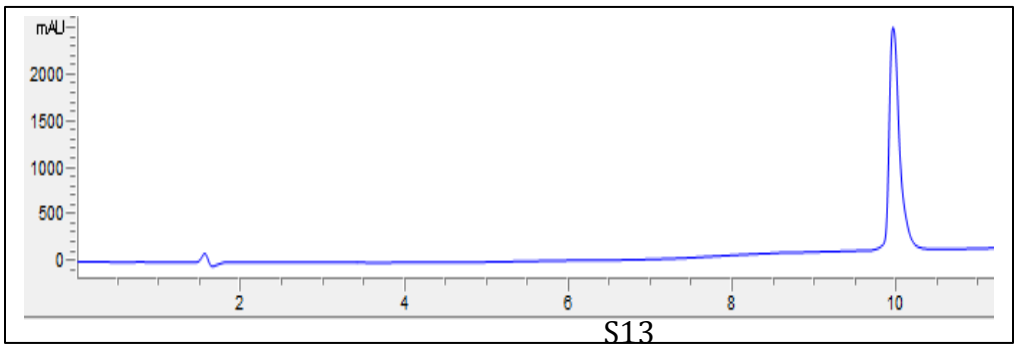

MLL6

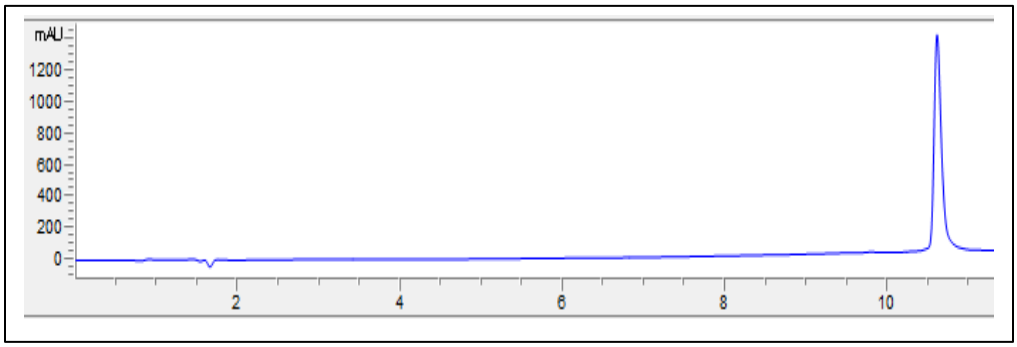
mAU
1200
1000
800
600
400
200
0
2
4
6
8
10

C*→A

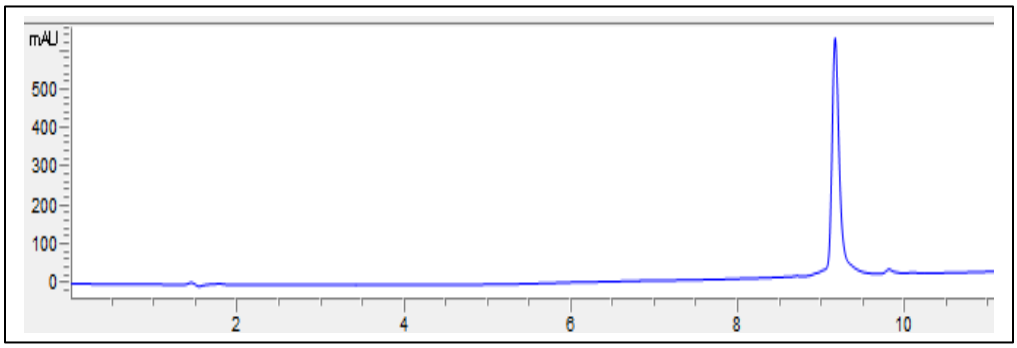
mAU
500
400
300
200
100
0
2
4
6
8
10

F*→A

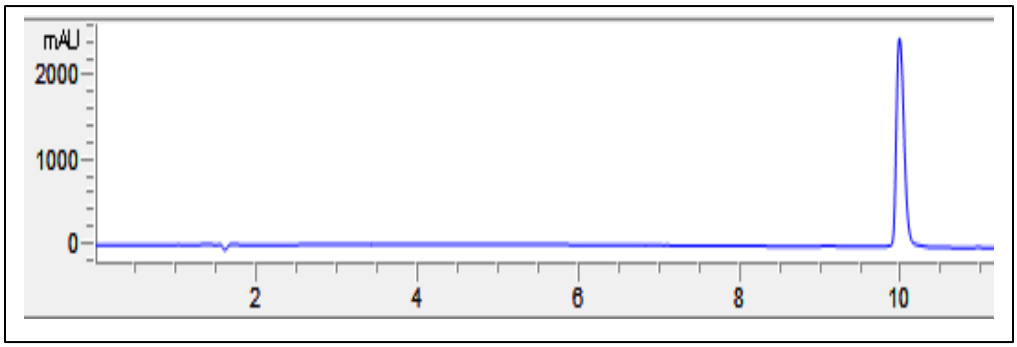
mAU
2000
1000
0
2
4
6
8
10

I→A

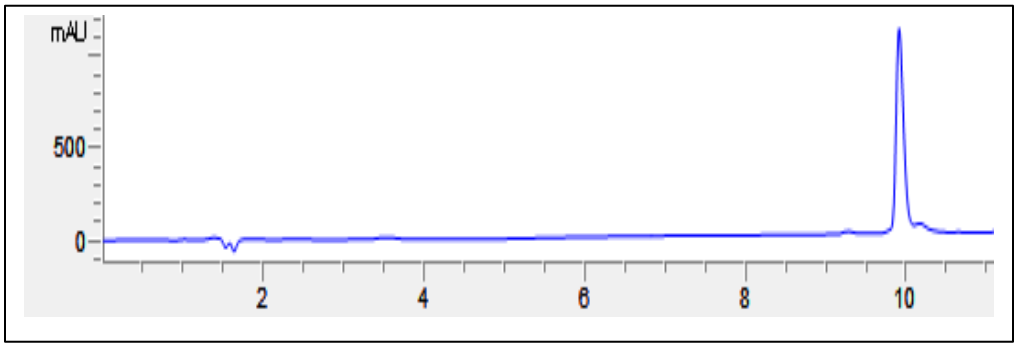
mAU
500
0
2
4
6
8
10

Y→A

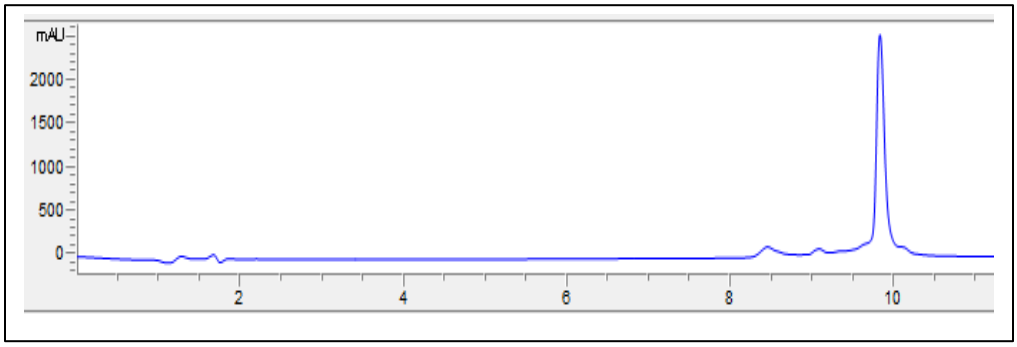
mAU
2000
1500
1000
500
0
2
4
6
8
10

OH→NH_2

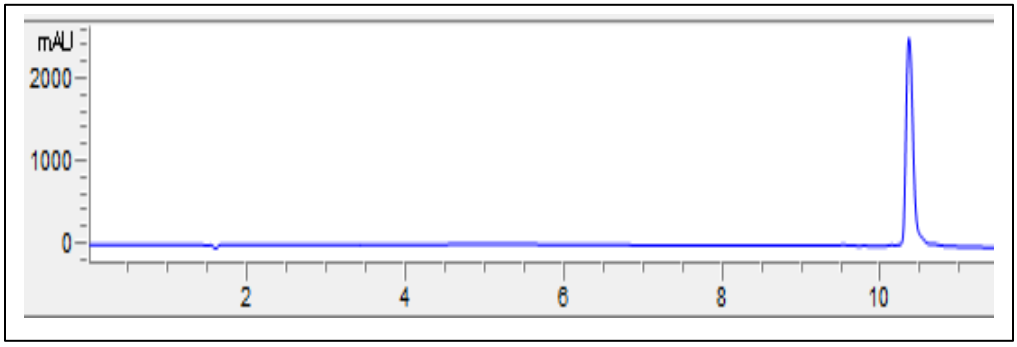
mAU
2000
1000
0
2
4
6
8
10

Circular Dichroism Studies:
CD spectra for MLL 1-6 were recorded using AVIV 202SF CD spectrometer in 1 mm cells at 25.00 °C, 1.000 nm bandwidth slits, from 260.00 nm to 185.00 nm with increments of 0.500 nm, averaging time of 0.500 seconds, with 4 scans per sample. The CD spectrum for WT-MLL was recorded using a JASCO J-1500 CD Spectrometer under the same conditions except with 0.500 nm bandwith slits and 5 scans per sample. Baselines were subtracted from analogous conditions as that from samples. Each sample was prepared at 50 µM in 0.1X PBS (13.7 mM NaCl, 0.27 mM KCl, 1 mM Na_2HPO_4, 0.18 mM KH_2PO_4, pH 7.4) as performed in Joy, S. T., *et al*. [15]

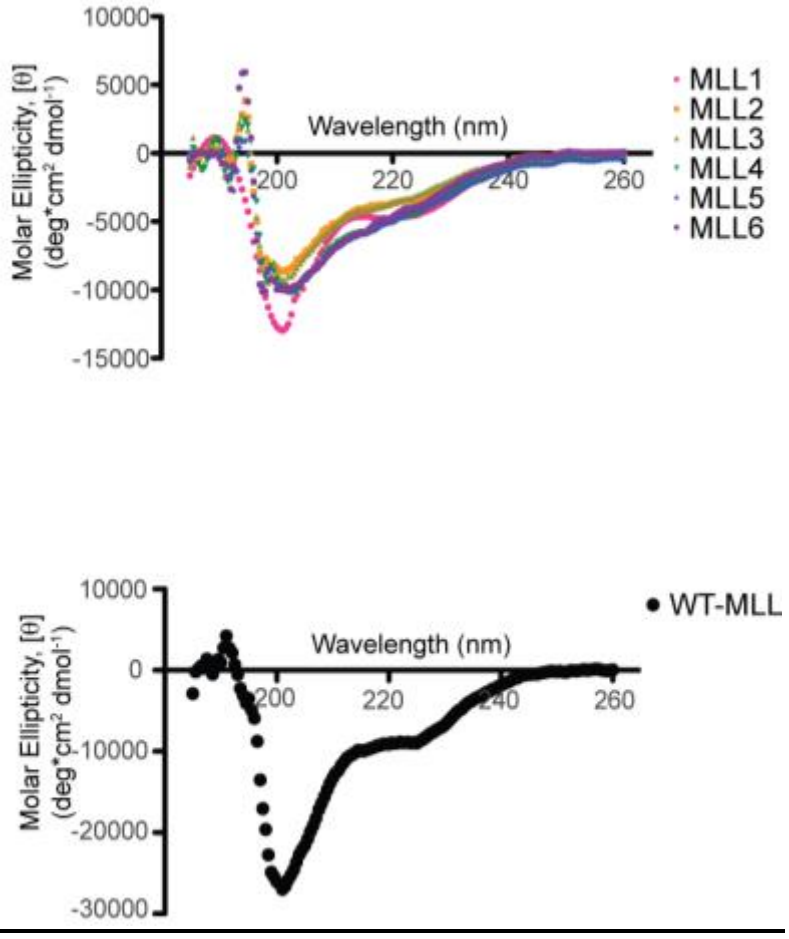

Fig S7: CD data for MLL1-6 (Top) and WT-MLL (Bottom).

Protein Expression and Purification

His-KIX plasmid was transformed into electrocompetent Rosetta™(DE3)pLysS *E. coli* cells. Cells were grown on agar plates containing ampicillin overnight. A single colony was used to inoculate a 50 mL LB overnight growth supplemented with ampicillian (100 μg/mL) and chloramphenicol (25 μg/mL). A total of 2.5 L of LB containing ampicillian (100 μg/mL) and chloramphenicol (25 μg/mL) was seeded with the overnight culture and incubated at 37 °C at 250 RPM until OD_{600} reached 0.6. The cells were induced with 0.5 mM of IPTG at 25 °C at 250 RPM. Cells were harvested 4 hours after induction by centrifugation at 4000 RPM for 35 minutes at 4 °C and the supernatant was discarded. Pellets were stored in the -80 °C freezer until purification. The cells were resuspended in lysis buffer: 300 mM NaCl, 50 mM Na_2HPO_4, 10 mM Imidizole, β-mercaptoethanol (0.7 μL/mL of buffer), EDTA-free protease inhibitors (Roche), pH 7.2. The solution was sonicated and centrifuged at 20,000 RPM for 20 minutes at 4 °C. The resultant supernatant containing His-KIX was applied to washed and equilibrated HisPur™ Ni-NTA Resin (ThermoScientific) for 1-2 hours rocking at 4 °C. The flow through was discarded and the column was washed with wash buffer: 50 mL, 300 mM NaCl, 50 mM Na_2HPO_4, 30 mM Imidizole, pH 7.4. The protein was eluted using a gradient of 60 – 300 mM imidazole in 300 mM NaCl, 50 mM Na_2HPO_4, pH 7.4. Fractions were checked by SDS-PAGE gel electrophoresis and pure fractions were pooled and dialyzed into PBS buffer pH 7.4 (137 mM NaCl, 2.7 mM KCl, 10 mM Na_2HPO_4, 1.8 mM KH_2PO_4) to remove imidazole. 10% glycerol was added to the combined pure protein fractions and snap frozen with liquid nitrogen before storing at -80 °C until use.

Fluorescence Polarization Assays:

Sample Preparation:

Concentrations of protein and peptide samples were determined using Nanodrop 2000c (ThermoScientific).

A) Direct Binding Experiments:

The relative affinity of Flu-tagged MLL sequences was determined using a fluorescence polarization assay. Experiments were performed in triplicate in a 96-well plate format. His-KIX was concentrated in 10% glycerol in PBS (137 mM NaCl, 2.7 mM KCl, 10 mM Na_2HPO_4, 1.8 mM KH_2PO_4, pH 7.4) using Amicon ® Ultra Centrifugal filters according to the manufacturer's protocol. Pluronic F-127 (Sigma) was added to a final concentration of 0.1% in each experiment. The protein was serially diluted so that the final concentration of His-KIX in each experiment ranged from ~60 μM – 0. All Flu-tagged peptides were dissolved in the same buffer as the protein to a concentration of 300 nM so that in each well the final concentration of Flu-tagged peptide was 15 nM. Each plate incubated for 40 minutes at room temperature and was read on a DTX 880 Multimode Detector (Beckman) at 25 °C with excitation of 485 nm and emission of 525 nm. Raw values were fit to a sigmoidal dose-response nonlinear regression model in GraphPad Prism 5.0. to obtain the EC_{50} value. The binding affinities (K_D) for each peptide was determined using the following equation as performed in Lao, *et al.* [16] The following equation from [17] was used:

$$K_D = (R_T \times (1-F_{SB}) + L_{ST} \times F_{SB}^2)/F_{SB} - L_{ST} \quad \textbf{(1)}$$

R_T = EC_{50} value determined by prism
F_{SB} = fraction bound = 0.5 (in the case of EC_{50})
L_{ST} = total concentration of Flu-peptide = 15 nM (for all experiments)

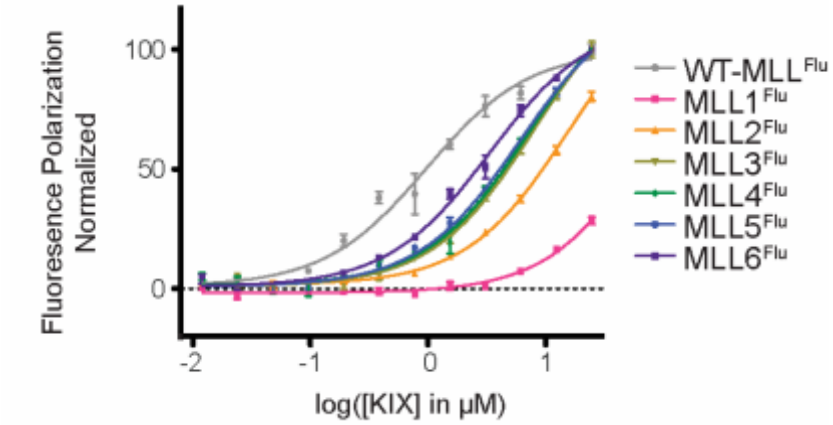

Fig S8: Direct binding data for wild type and MLL1-6 compounds. The calculated Hill slope (from Prism software) for the binding curves is 1.0-1.2.

B) Competition Binding Experiments:
Inhibition studies were performed using WT-MLL^{Flu}, His-KIX and unlabeled MLL analogues. All studies were performed in triplicate in a 96 well plate format and detected as done above for direct binding studies with a final concentrations of 10% glycerol and 0.1% Pluronic F-127 (Sigma) in PBS, pH 7.4. The MLL analogues were dissolved in DMSO to a final concentration of ~40 mM and serially diluted so that the concentration in each well ranged from 2 mM – 0, and so that the final concentration of DMSO in the well was 5%. As performed in direct binding studies, the WT-MLL^{Flu} stock was 300 nM so that in each well its final concentration was 15 nM. A blank direct binding study was performed with WT-MLL^{Flu} and DMSO with no compound present to determine the concentration of His-KIX at 65% saturation. In competition experiments, 15 nM of WT-MLL^{Flu}, His-KIX at 65% saturation were added to each well and the varying amounts of MLL analogues in DMSO were added to each well. Samples incubated at room temperature for 1 hour before using the plate reader. The detection was read with the same parameters as done in the direct binding studies. The competition binding affinities (K_I) for each peptide was determined using the following equation as performed in Lao, *et al*. [16] The following equation from [17] was used:

$$K_I = K_D * F_{SB} * ((L_T/L_{ST} * F_{SB} - (K_D + L_{ST} + R_T) * F_{SB} + R_T)) - 1/(1 - F_{SB})) \qquad \textbf{(2)}$$

K_D = K_D of WT-MLL^{Flu} to His-KIX from equation Direct Binding **(1)**
F_{SB} = Fraction of WT-MLL^{Flu} bound to His-KIX at EC_{50}
L_T = Total concentration of WT-MLL^{Flu}
L_{ST} = EC_{50} of peptide from competition curve using equation **(1)** as determined by Prism
R_T = Total concentration of His-KIX protein

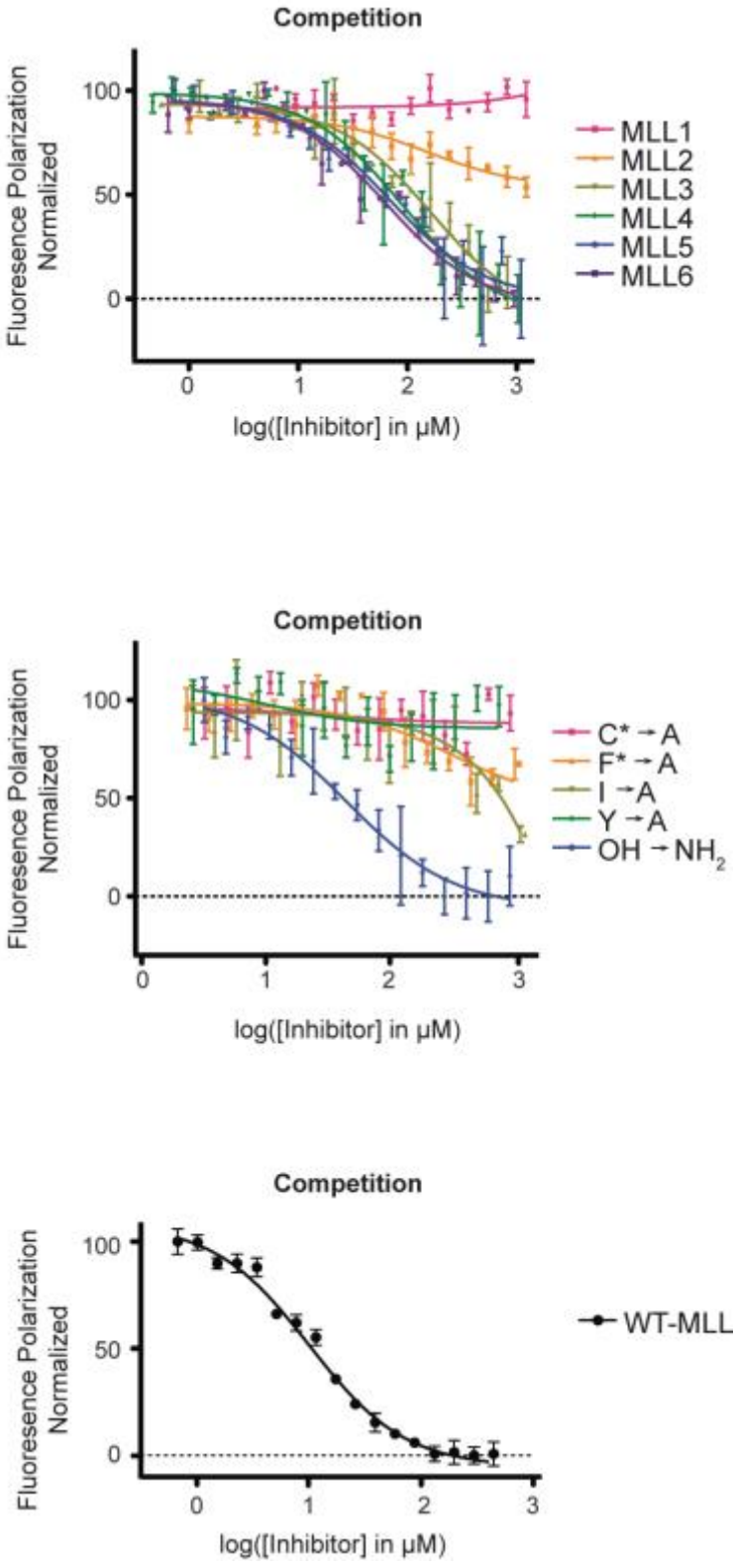

Fig S9: Competition binding experiments with unlabeled peptides. Top: MLL 1-6, Middle: alanine scanning data of MLL6. Bottom: WT-MLL.

Supporting References:

(1) Pettersen, E. F.; Goddard, T. D.; Huang, C. C.; Couch, G. S.; Greenblatt, D. M.; Meng, E. C.; Ferrin, T. E. *J. Comput. Chem.* **2004**, *25*, 1605.
(2) Brüschweiler, S.; Konrat, R.; Tollinger, M. *ACS Chem. Biol.* **2013**, *8*, 1600.
(3) De Guzman, R. N.; Goto, N. K.; Dyson, H. J.; Wright, P. E. *J. Mol. Biol.* **2006**, *355*, 1005.
(4) Rooklin, D. W.; Wang, C.; Katigbak, J.; Arora, P. S.; Zhang, Y. *J. Chem. Inf. Model* **2015**, *51*, 150730170651001.
(5) Gfeller, D.; Michielin, O.; Zoete, V. *Nucl. Acids Res.* **2013**, *41*, D327.
(6) Pettersen, E. F.; Goddard, T. D.; Huang, C. C.; Couch, G. S.; Greenblatt, D. M.; Meng, E. C.; Ferrin, T. E. *J. Comput. Chem.* **2004**, *25*, 1605.
(7) Case, D. A.; Babin, V.; Berryman, J. T.; Betz, R. M.; Cai, Q.; Cerutti, D. S.; Cheatham, T. E.; Darden, T. A.; Duke, R. E.; Gohlke, H.; Goetz, A. W.; Gusarov, S.; Homeyer, N.; Janowski, P.; Kaus, J.; Kolossváry, I.; Kovalenko, A.; Lee, T. S.; LeGrand, S.; Luchko, T.; Luo, R.; Madej, B.; Merz, K. M.; Paesani, F.; Roe, D. R.; Roitberg, A.; Sagui, C.; Salomon-Ferrer, R.; Seabra, G.; Simmerling, C. L.; Smith, W.; Swails, J.; Walker, R. C.; Wang, J.; Wolf, R. M.; Wu, X.; Kollman, P. A. *AMBER 2014* University of California, San Francisco, 2014.
(8) Maier, J. A.; Martinez, C.; Kasavajhala, K.; Wickstrom, L.; Hauser, K. E.; Simmerling, C. *J. Chem. Theor. Comput.* **2015**, *11*, 3696.
(9) Khoury, G. A.; Smadbeck, J.; Tamamis, P.; Vandris, A. C.; Kieslich, C. A.; Floudas, C. A. *ACS Synth. Biol.* **2014**, *3*, 855.
(10) Hou, X. B.; Rooklin, D.; Fang, H.; Zhang, Y. K. *Sci Rep-Uk* **2016**, *6*.
(11) Gotz, A. W.; Williamson, M. J.; Xu, D.; Poole, D.; Le Grand, S.; Walker, R. C. *J. Chem. Theor. Comput.* **2012**, *8*, 1542.
(12) Salomon-Ferrer, R.; Gotz, A. W.; Poole, D.; Le Grand, S.; Walker, R. C. *J. Chem. Theor. Comput.* **2013**, *9*, 3878.
(13) Subiros-Funosas, R.; El-Faham, A.; Albericio, F. *Tetrahedron* **2011**, *67*, 8595.
(14) Majmudar, C. Y.; Hojfeldt, J. W.; Arevang, C. J.; Pomerantz, W. C.; Gagnon, J. K.; Schultz, P. J.; Cesa, L. C.; Doss, C. H.; Rowe, S. P.; Vasquez, V.; Tamayo-Castillo, G.; Cierpicki, T.; Brooks, C. L., 3rd; Sherman, D. H.; Mapp, A. K. *Angew. Chem. Int. Ed.* **2012**, *51*, 11258.
(15) Joy, S. T.; Arora, P. S. *Chem. Commun.* **2016**, *52*, 5738.
(16) Lao, B. B.; Drew, K.; Guarracino, D. A.; Brewer, T. F.; Heindel, D. W.; Bonneau, R.; Arora, P. S. *J. Am. Chem. Soc.* **2014**, *136*, 7877.
(17) Roehrl, M. H.; Wang, J. Y.; Wagner, G. *Biochemistry* **2004**, *43*, 16056.